Kinetic and structural evidence for specific DMSO interference with reversible binding of uncharged bis-oximes to hAChE and their reactivation kinetics of OP-hAChE.

Dora Kolić[a], Oksana Gerlits[b], Megan Kucharski[c], Lukas Gorecki[d,e], Nichole Joiner[c], Andrey Kovalevsky[f] and Zoran Radić[c*]

[a] Institute for Medical Research and Occupational Health, HR-10001 Zagreb, Croatia
[b] Department of Natural Sciences, Tennessee Wesleyan University, Athens, TN 37303, USA
[c] Skaggs School of Pharmacy and Pharmaceutical Sciences, University of California San Diego, La Jolla, CA 92093-0650, USA
[d] Department of Toxicology and Military Pharmacy, Military Faculty of Medicine, University of Defence, 500 01 Hradec Kralove, Czech Republic
[e] Biomedical Research Center, University Hospital Hradec Kralove, 500 05 Hradec Kralove, Czech Republic
[f] Neutron Scattering Division, Oak Ridge National Laboratory, Oak Ridge, TN 37831, USA

*Correspondence: Zoran Radić, email: zradic@ucsd.edu

Abstract

The structural basis of inhibitory effect of organic solvent dimethyl sulfoxide (DMSO) on human acetylcholinesterase (EC 3.1.1.7; hAChE) was inferred from the effect of DMSO on kinetics of reversible inhibition of uncharged, heterocyclic bis-oximes to hAChE, from DMSO effect on rates of reactivation of inactive organophosphate (OP)-hAChE conjugates by bis-oximes and by X-ray structures of bis-oxime and DMSO binding to hAChE. The reversible inhibition constant of DMSO for hAChE in 0.1 M phosphate buffer pH 7.4 at 22 °C, was K_i= (0.32 ± 0.04) % (or 45 ± 5 mM). The K_i of the bis-oxime LG-703 for hAChE was 3.2-fold larger in 1% DMSO, consistent with direct competition between LG-703 and DMSO. The X-ray structure of the LG-703*hAChE complex (PDB ID: 6U3P) shows DMSO and LG-703 bound to individual hAChE monomers, LG-703 in the chain A and DMSO in the chain B. In the co-crystallization both small molecules were present at a similar excess over their corresponding K_i values for hAChE (7.8-fold for DMSO and 6.5-fold for LG-703) and formation of two different complexes (DMSO*hAChE and LG-703*hAChE), in the same crystal, appears consistent with inhibition kinetics. Furthermore, rates of reactivation of paraoxon-inhibited hAChE (POX-hAChE) and of VX-hAChE by LG-703 and by a novel heterocyclic bis-oxime LG-1922 were reduced 2 – 3-fold in DMSO, consistent with observation of the active-center-bound DMSO molecules in the newly solved structure of the LG-1922*POX-hAChE complex presented here and in our POX-hAChE structure (PDB ID: 8DT2) showing obstruction of the reactivator access to the conjugated P atom.

Keywords: DMSO, acetylcholinesterase inhibition, heterocyclic bis-oximes, acetylcholinesterase reactivation, organophosphorus compounds, VX, paraoxon, antidotes, organic solvent

1. Introduction

Intoxication by organophosphates (OPs) leads to covalent inhibition of acetylcholinesterase (AChE; EC 3.1.1.7), the key enzyme of cholinergic neurotransmission, resulting in harmful accumulation of acetylcholine in nervous tissue that can lead to cholinergic crisis and result in death [1,2]. Nucleophilic antidotes that reactivate covalent OP-hAChE conjugates are the only therapeutic approach that targets the actual cause of OP toxicity. The worldwide approved reactivating antidotes are all cationic pyridinium-based oxime derivatives with access restricted to the circulation and peripheral nervous system. These oximes are incapable of traversing the Blood-Brain-Barrier and reaching AChE inhibited in the central nervous system. Design of novel uncharged reactivating oximes has therefore been one of notable directions for their significant therapeutic improvement. Molecules of uncharged oximes, by virtue of the absence of an explicit (permanent) charge in their structures, are frequently not easily soluble in the aqueous medium and for initial *in vitro* functional screening require dissolution in organic solvents such as dimethyl sulfoxide (DMSO). A presence of DMSO, or another organic solvent, is therefore common in the initial functional screening of uncharged antidotes [3–8].

At concentrations below 0.5% v/v, DMSO has generally little effect on the catalytic activity of hAChE [9]. In the presence of DMSO concentrations of 1% or higher, however, DMSO and other solvents have pronounced inhibitory effect on catalytic activity of AChEs [9, 10, 11]. Furthermore, the kinetics of oxime reactivation of OP-hAChE has been observed to yield somewhat different values of reactivation rate constants ([3,12]; Table S1) compared to that in DMSO absence.

In this study we have quantitatively evaluated the effect of DMSO on the kinetics of interaction of our novel uncharged bis-oximes with hAChE and explored specific sites of DMSO binding in X-ray structures of their reversible complexes with hAChE. Reversible inhibition constants of hAChE by bis-oximes were evaluated in the absence and presence of DMSO as well as the reversible inhibition constant of the DMSO*hAChE complex. Reactivation rate constants of hAChE covalently inhibited by organophosphate insecticide paraoxon and by nerve agent VX were evaluated for novel uncharged bis-oximes in the absence and in the presence of DMSO.

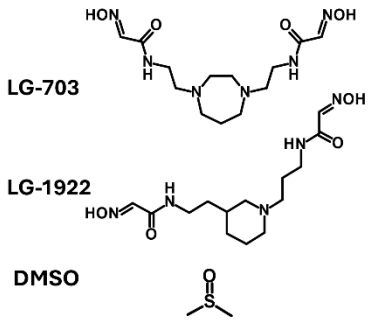

Figure 1. Structures of heterocyclic bis-oximes LG-703 and LG-1922 and of dimethyl sulfoxide (DMSO).

Finally, in addition to providing the analysis of DMSO binding in the previously solved X-ray structure of a reversible complex of the bis-oxime LG-703 with native hAChE (PDB ID: 6U3P; [3]) we have now solved new X-ray structures of a novel heterocyclic bis-oxime LG-1922 (Fig.1) in the complex with hAChE and with POX-hAChE conjugate. The latter structure shows a clear evidence of specific binding sites of DMSO molecules, in the complex.

2. Materials and methods

2.1. Preparation of hAChE and bis-oxime reactivators

Monomeric form of human AChE truncated at the C-terminal amino acid position 547 was expressed in Gnt1- HEK293 cells and purified using N-terminal FLAG tag on the anti-FLAG affinity column by proteolytic elution, as described before [13].

DMSO was purchased from Fisher bioreagents (>99.7%; BP231-100, LOT 245004).

Bis-oxime **LG-703** was prepared as described before [3]. The synthesis of bis-oxime **LG-1922** was conducted in a similar fashion, although it is presented here for the first time (see Scheme 1). ~~Initially,~~ The starting material, 2-(piperidin-3-yl)acetonitrile hydrochloride (**1**), was *N*-alkylated by 3-bromopropionitrile in the presence of *N*,*N*-diisopropylethylamine (DIPEA). The reduction of bis-nitrile product **2** was achieved by Raney-Nickel under hydrogen atmosphere, resulting in the formation of bis primary amine compound **3**. Finally, the ensuing reaction of **3** with ethyl (2*E*)-2-(hydroxyimino)acetate, prepared according to previously described procedure [4], led to desired product **LG-1922** as racemic mixture.

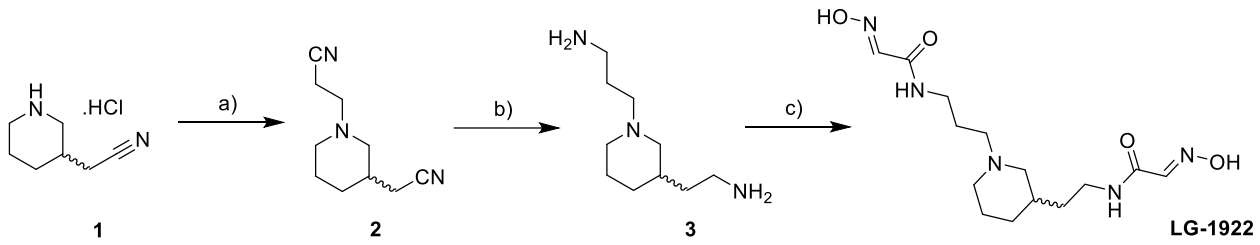

Scheme 1. Chemical synthesis of bis-oxime **LG-1922**. Reagents and conditions: a) 3-bromopropionitrile, DIPEA, THF/methanol (4:1), Ar, room temperature (RT), 48 hours; b) Raney-Nickel, methanol, H_2, RT, 14 hours; c) ethyl (2*E*)-2-(hydroxyimino)acetate, ethanol, Ar, 80 °C, 72 hours.

2.2. Reversible inhibition of hAChE by DMSO

Catalytic activity of hAChE in 0.1 M Phosphate buffer, pH 7.4 supplemented with 0.01% BSA was measured spectrophotometrically at 22 °C using Ellman assay [14]. The activity assay mixture contained 30 µL of the Ellman thiol reagent DTNB (10 mM stock in buffer), 950 µL of the buffer, 10 µL of acetylthiocholine (ATCh; 100 mM or appropriate stock in water) and 10 µL of purified hAChE (~10 nM). The direct inhibitory effect of DMSO was measured by substituting either 5 µL or 10 µL of the buffer in the assay mixture with DMSO. The enzyme activity was measured at 0.050 mM, 0.10 mM, 0.20 mM, 0.30 mM and 0.40 mM ATCh concentrations in the 1.0 mL assay mixture, in the absence (v_0) and presence of DMSO (v_i). All activity assay measurements were done in at least duplicate. At each ATCh concentration value of the $K_{i,app} = [DMSO]*v_i/(v_0-v_i)$ was calculated and plotted vs. [ATCh] to yield a Hunter-Downs plot [13]. Values of intercepts on the ordinate (K_i) and on the abscissa ($K_{[ATCh]}$) were obtained by linear regression using equation [15]:

$$K_{i,app} = K_i \cdot \left(1 + [ATCh]/K_{[ATCh]}\right) \quad \text{(Eq. 1)}$$

2.3. The effect of DMSO on reversible inhibition of hAChE by LG-703

The inhibition of hAChE by the uncharged heterocyclic bis-oxime LG-703 (Fig.1.) was measured as described for DMSO in the section 2.2. using 0.10 mM, 0.2 mM, 0.50 mM and 1.0 mM final concentrations of LG-703 in the assay mixture. Stock solutions of 100 mM LG-703 prepared in either water (by titration with ~ 2 µL of 36 % HCL per 100 µL of 100 mM LG-703) or in DMSO, were used in inhibition assays. The resulting $K_{i,app}$ = [DMSO]*v_i/(v_0-v_i) values were plotted in the Hunter-Downs plot for each LG-703 concentration. The reversible inhibition constant of LG-703 (K_i^{LG-703}) in the absence of DMSO was determined by linear regression using Eq. 1. and in the presence of DMSO using the equation:

$$K_{i,app,DMSO} = K_i^{LG-703} \cdot (1 + [DMSO]/K_i) + \left(K_i^{LG-703}/K_{[ATCh]}\right) \cdot [ATCh] \quad \text{(Eq. 2)}$$

2.4. The effect of DMSO on reactivation of OP-hAChEs by LG-703 and LG-1922

The covalent conjugate VX-hAChE identical to the one resulting from the inhibition by the nerve agent VX, was prepared using low toxicity Flu-MP analogue of the nerve agent VX [16]. Inhibition of hAChE by Flu-MP results in the VX-hAChE covalent conjugates identical to the one formed upon inhibition with the much more ~~volatile~~ hazardous nerve agent VX. Four to ten-fold stoichiometric excess of Flu-MP or paraoxon was used to inhibit hAChE (~20 µM) for several minutes at room temperature resulting in >99 % loss of catalytic activity, to ensure homogeneous inhibition by the more potent S_P enantiomer of the Flu-MP. Excess unreacted Flu-MP was removed from the inhibition mixture by Sephadex G-50 separation on two consecutive spin columns (Bio-Spin 6 Tris columns, BioRad, Hercules, CA). Time-dependent recovery of hAChE activity was monitored spectrophotometrically [12] in 0.1 M Phosphate buffer, pH 7.4 (containing 0.01 % BSA) upon addition of LG bis-oximes at 37 °C. The first order reactivation rate constant (k_{obs}) for each (oxime + OP-hAChE conjugate) combination was calculated by nonlinear regression (of %Act=A*(1-$e^{(k_{obs}*t)}$). The dependence of reactivation rates on oxime concentrations and determination of maximal reactivation rate constant k_2, Michaelis-Menten type constant K_{ox}, and the overall second order reactivation rate constant k_r were conducted as previously described [17]. The effect of DMSO on reactivation rate constants of POX-hAChE within the reactivation mixture was evaluated by using LG-703 stock solutions prepared in either water or in DMSO. With the DMSO stock solution that resulted in 0.5 %, 1.0 % and 1.5 % DMSO in the reactivation mixture. In all other reactivation experiments (LG-703 + VX-hAChE; LG-1922 + POX-hAChE and LG-1922 + VX-hAChE) LG-703 and LG-1922 stock solutions prepared in water were used and DMSO was added into reactivation mixture at the 3 % final concentration or not added to the reactivation mixture, at all.

2.5. X-ray structures of LG-1922 in reversible complexes with native hAChE and with POX-hAChE conjugate

For crystallization, hAChE was dialyzed in 10 mM NaCl, 10 mM HEPES, pH 7, and concentrated to 8 – 9 mg/mL. The solution of hAChE was combined with a stock solution of reactivator LG-1922 (50 mM in DMSO) in a molar ratio of 1:5 to obtain the corresponding binary complex. The mixture was then kept on ice for about 1 hour prior to setting up crystallization trays. Crystals were grown by vapor diffusion at 10 °C in sitting drop microbridges (Hampton Research, Aliso Viejo, CA). Well solutions contained 100 mM HEPES pH 7.5, 100 mM KNO_3, and 11 % PEG 3350. To obtain the LG-1922 complex with POX-hAChE conjugate, crystals of the binary complex, LG-1922*hAChE, were soaked in the solution of POX. Specifically, 3 µL of 100 mM POX solution in ethanol were diluted with 400 µL of the solution from a chosen crystallization well. The soaking drop containing 10 µL of the corresponding POX solution was supplemented with 0.5 µL of LG-1922 stock solution. All crystals were soaked for 4 min at RT (~22 °C).

For all complexes reported here, X-ray crystallographic data were collected from frozen crystals at 100 K. Prior to data collection crystals were subjected to two very brief consecutive soaks in the cryoprotectant solutions, first in 12.5 % glycerol followed by 25 % glycerol, and then flash cooled by plunging into liquid nitrogen. Diffraction data were collected from a single crystal for each complex on the ID19 beamline at SBC-CAT using a Pilatus3 X 6M detector at the Advanced Photon Source (APS). X-ray diffraction data were integrated and scaled using the HKL3000 software suite [18]. The structures were solved by molecular replacement using the CCP4 suite [19]. The structure of the LG-703*hAChE-RS194B complex (PDB ID 6U3P) [3] was used as a starting model with all waters removed. Refinement was performed using the *phenix.refine* program in the *PHENIX* [20, 21] suite and the resulting structure analyzed with molprobity [22]. The structures were built and manipulated with program *Coot* [23,24]. A summary of the crystallographic data and refinement is given in Table S2. Crystallographic data have been deposited to the PDB with the following codes: 9OMS for LG-1922*hAChE, and 9OMT for LG-1922*POX-hAChE.

3. Results and discussion

3.1. The effect of DMSO on reversible inhibition of hAChE by LG-703

The presence of DMSO in the hAChE catalytic activity assay mixtures showed reversible, concentration dependent interaction with the enzyme (Fig.1.) resulting in inhibition of its activity consistent with K_i = 0.32 % or 45 mM for DMSO (Fig.1A). Interaction with substrate ATCh was largely competitive as inferred from the linearity of the plot (Fig.1A) and sub-mM values of X-axis intercepts ($K_{[ATCh]}$) similar to K_m for ATCh [15]. The value of K_i was reasonably close to those previously determined for hAChE (88.7 mM; [9]) and for Electrophorus electricus AChE (80 mM; [10]) considering the difference in experimental conditions and the source of AChE. The bis-oxime LG-703 inhibited hAChE, in the absence of DMSO, in a less competitive manner vs. ATCh, indicated by the notably larger X-axis intercept and with the K_i^{LG-703} = 250 µM (Fig.1B).

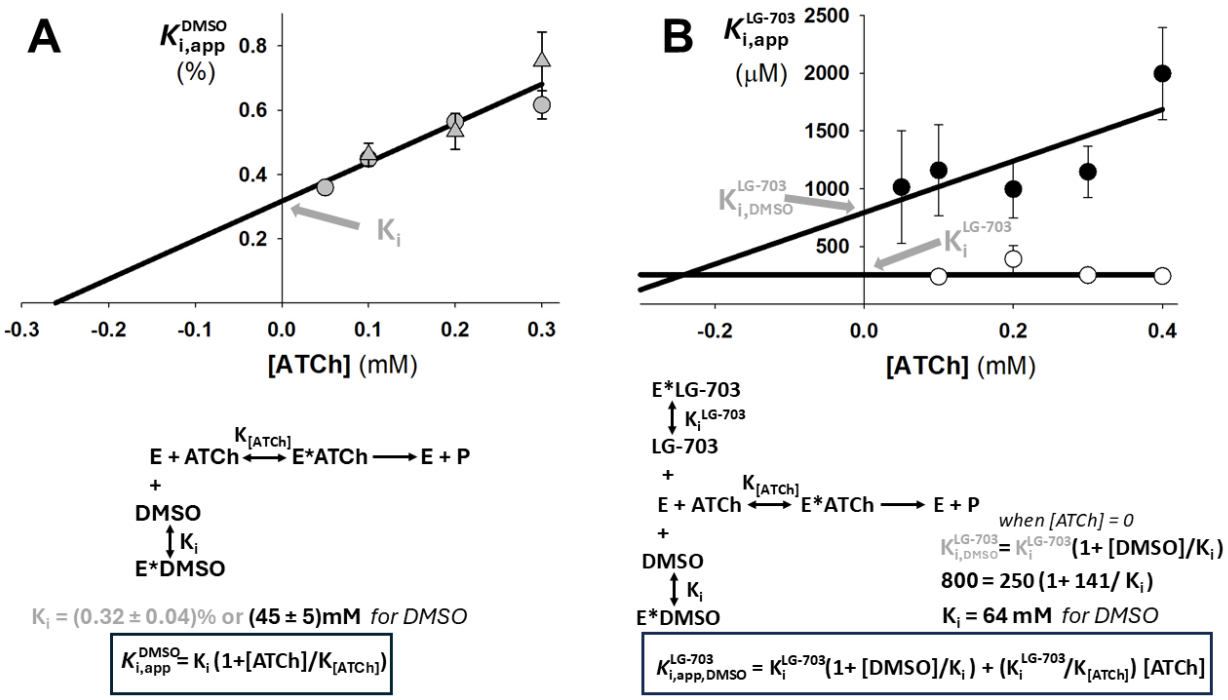

Figure 2. Hunter-Downs plots of reversible inhibition of human AChE by **A)** 0.5 % DMSO (circles) and 1 % DMSO (triangles) with standard error of $K_{i,app}$ replicates shown for the each of two DMSO concentrations and **B)** 0.10 mM, 0.2 mM, 0.50 mM and 1.0 mM concentrations of LG-703 in the absence (white circles) or presence (black circles) of DMSO. Standard errors show the $K_{i,app}$ variability within four LG-703 concentrations at each ATCh concentration. Corresponding kinetic schemes show reversible interaction of DMSO and LG-703 with the substrate ATCh turnover by AChE (E). Equations were derived assuming equilibrium conditions [15].

In the presence of DMSO interaction of LG-703 with ATCh assumed a clearly competitive character (consistent with reduction of the X-axis intercept value) but inhibition was several-fold weaker, resulting in $K_{i,DMSO}^{LG-703}$ = 800 μM (Fig.1B). This reduction in inhibition (or increase in the value of $K_{i,DMSO}^{LG-703}$ vs. value of K_i^{LG-703} (Fig.1B) was consistent with value of K_i for DMSO of 64 mM (Fig.1B), very close to the value of 45 mM derived from direct inhibition of hAChE by DMSO. The similarity is consistent with proposed kinetic mechanism and scheme for interaction of DMSO with LG-703 and ATCh in binding to hAChE (Fig.1B). Thus, DMSO inhibits hAChE reversibly, in a concentration-dependent manner competitive with ATCh, with K_i = 0.32 % or 45 mM. The inhibitory DMSO binding to hAChE appears quantitatively competitive with reversible inhibition of hAChE by heterocyclic bis-oxime LG-703, increasing its inhibition constant by the factor of 800/250 = 3.2 (Fig. 2B) consistent with the value of K_i determined directly for DMSO.

3.2. The effect of DMSO on reactivation of OP-hAChEs by LG-703 and LG-1922

Interaction of DMSO with OP-hAChE conjugates significantly affected kinetics of their reactivation by heterocyclic bis-oximes LG-703 and LG-1922 (Fig.1). The time-courses of reactivation of both POX-hAChE and VX-hAChE were slowed-down in the presence of DMSO (Fig.3.) resulting in the altered concentration dependence of the reactivation by each of the two bis-oximes (Fig.3B-D).

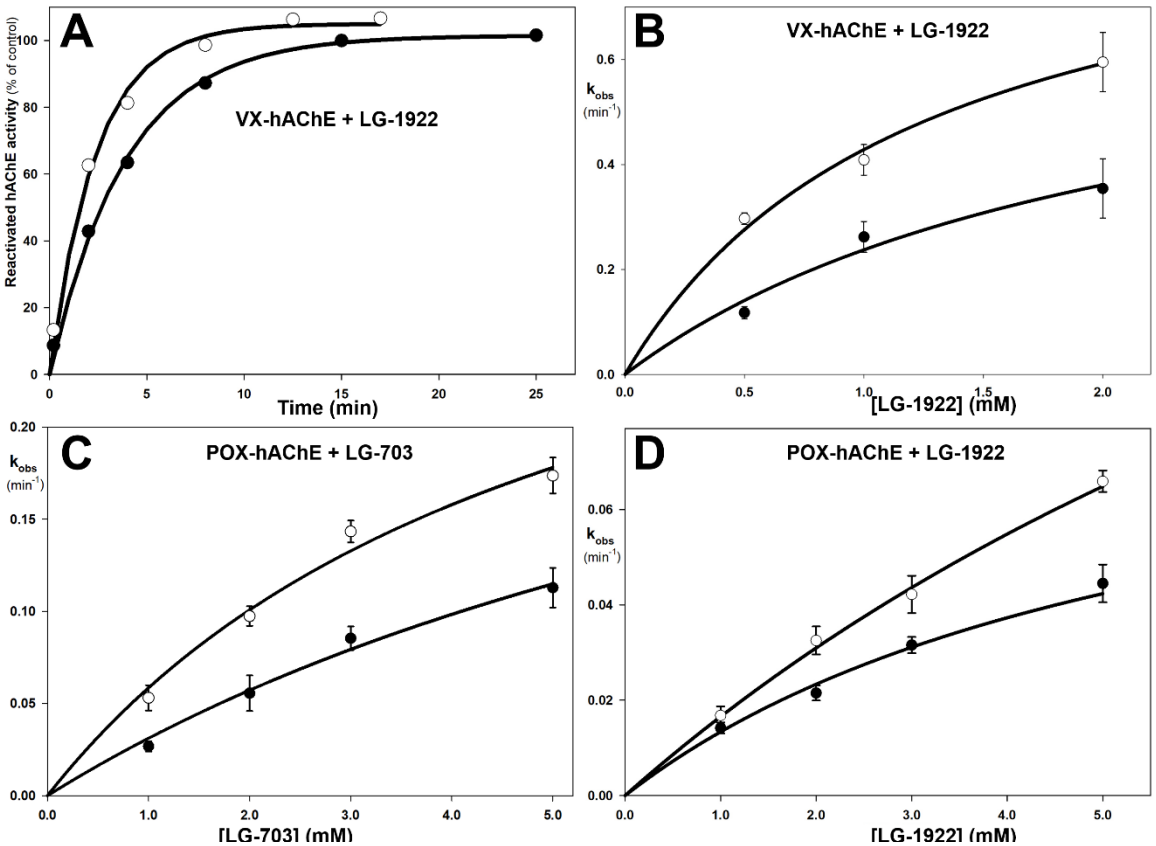

Figure 3. The effect of DMSO on kinetics of nucleophylic reactivation of OP-hAChE conjugates by heterocyclic bis-oximes. **A)** Time-course of reactivation of VX-hAChE by 1 mM LG-1922 in 3 % DMSO (black circles) and in its absence (white circles). **B)** Concentration dependence of VX-hAChE reactivation by LG-1922 in 3 % DMSO (black circles) and in its absence (white circles). **C)** Concentration dependence of POX-hAChE reactivation by LG-703 in DMSO (black circles) and in its absence (white circles). **D)** Concentration dependence of POX-hAChE reactivation by LG-1922 in 3 % DMSO (black circles) and in its absence (white circles). Error bars represent standard errors for the first order reactivation rate constants k_{obs} determined at each bis-oxime concentration from nonlinear regression of reactivation time-course curves.

Values of all reactivation rate constants evaluated from curves of concentration dependences (Fig.3.) were affected by DMSO as summarized in Table 1.

Table 1. The effect of DMSO on kinetic constants of reactivation by heterocyclic bis-oximes.[a]

bis-oxime	DMSO	POX-hAChE			VX-hAChE		
		k_2	K_{ox}	k_r	k_2	K_{ox}	k_r
LG-703	none	0.36 ± 0.07	5.2 ±1.6	70 ± 9	3.7 ± 0.1	3.1 ± 0.1	1200 ± 10
	+	0.35 ± 0.18	10 ± 7	34 ± 6	4.0 ± 2.4	8.1 ± 6.0	490 ± 64
LG-1922	none	0.16 ± 0.04	6.6 ± 2.1	24 ± 2	0.96 ± 0.24	1.2 ± 0.7	770 ± 230
	+	0.092 ± 0.008	5.0 ± 0.7	18 ± 1	0.76 ± 0.21	2.2 ± 1.0	350 ± 78

[a]Maximal reactivation rate constant k_2 (min^{-1}), Michaelis-Menten type constant K_{ox} (mM), and the overall second order reactivation rate constant k_r (M^{-1} min^{-1}) were calculated by nonlinear regression from curves in Fig. 3 as previously described [12]. Given are standard errors obtained from nonlinear regression. Constants were evaluated from two or more experiments.

Overall, the presence of DMSO reduced values of the second order reactivation rate constants, k_r for all four tested reactions: LG-703 + POX-hAChE, LG-703 + VX-hAChE, LG-1922 + POX-hAChE and LG-1922 + VX-hAChE, in a statistically significant manner (Table 1). The reduction was more than two-fold in the VX-hAChE for both bis-oximes, and POX-hAChE for LG-703, while the presence of DMSO reduced values of k_r ~~only~~ by 25% in the reactivation of POX-hAChE by LG-1922. The reactivation by each of two bis-oximes was, thus, altered by DMSO for both OP-hAChE conjugates in a similar manner. ~~However,~~ The effect on the composite constant k_r ($k_r = k_2/K_{ox}$; [17]) of ~~VX-hAChE~~ POX-hAChE by LG-1922 ~~was affected by DMSO differently than that of POX-hAChE~~ was primarily in reduction of the k_2 constant i.e. in compromising the attack angle for nucleophilic attack in reactivation. That was consistent with a non-productive LG-1922 conformation revealed by our X-ray structures (Fig. 5). ~~Specifically, the majority of~~ Otherwise, reductions in values of the composite constant k_r ~~($k_r = k_2/K_{ox}$; [15]) for VX-hAChE~~ were consequence of about two-fold increase in K_{ox} values. The values of the maximal rate of reactivation k_2 remained largely unchanged (Table 1). That is consistent with simple competition between bis-oximes and DMSO where the presence of DMSO does not allow bis-oximes to bind to VX-hAChE close to conjugated P atom, in an orientation productive for nucleophilic in-line S_N2 reactivation. It is reminiscent of the competition between DMSO and ATCh that inhibits activity of the native hAChE (Fig. 1A). On the other hand, the small (25 %) reduction in the values of the constant k_r for POX-hAChE and LG-1922 was consequence of both, a smaller (by about 75 %) reduction in K_{ox} values and about two-fold decrease in the values of the maximal rate of reactivation k_2 (Table 1). In other words, bound DMSO ~~enhanced~~ allowed for binding of the bis-oxime reactivator to POX-hAChE, but in orientation that was non-productive for reactivation. ~~In that, essentially non-competitive reaction mechanism one has to assume that binding of DMSO induced a change of POX-hAChE protein conformation, resulting in smaller values for K_{ox}~~.

The possible reason for the limited difference in the mechanisms by which binding of DMSO affected reactivation of the two OP-hAChE conjugates may lie in their different size, and in the difference in the extent of the active center gorge impaction produced by their formation. Paraoxon inhibition forms diethylphosphorylated hAChE (POX-hAChE), while inhibition by VX forms smaller ethoxymethylphosphonylated hAChE (VX-hAChE). Of the two optical isomers in OP racemates the S_P isomer typically forms OP-hAChE about two orders of magnitude faster [25]. The resulting (>99 %) predominant, S_P chiral VX-hAChE conjugate has the methyl substituent on the phosphorus accommodated in the small volume of the hAChE acyl pocket and the larger ethoxy substituent facing the more spacious choline binding site of the enzyme. The covalently bound S_P-VX thus fits the available space of the hAChE active center well, without alterations of the main chain conformation and without significant changes in the conformation of the active center amino acid side-chains. That has been confirmed in numerous X-ray structures of VX-hAChE: 6U37, 6O5S, 6O66, 6CQT, 6CQW, 6CQZ [3,26,27]. On the other hand, covalently bound phosphorus in the POX-hAChE conjugate is symmetrically substituted with two ethoxy groups, one of which has to enter restricted space of the small acyl pocket and distort conformation of the acyl pocket loop in order to be accommodated. The significant acyl pocket loop distortion has been documented in several X-ray structures of POX-hAChE conjugates: 5HF5, 5HF8, 8DT2, 8DT4, 8DT5 [28,29]. The nature of the distortion differs in

different structures (Fig.4) and it also appears to be stabilized by reversibly bound DMSO in the structure 8DT2 ([29]; Fig.4). Conformations of the AP loop found in structures 5HF8 and 5HF5 would exclude DMSO from binding to the site identified in 8DT2 (Fig4.).

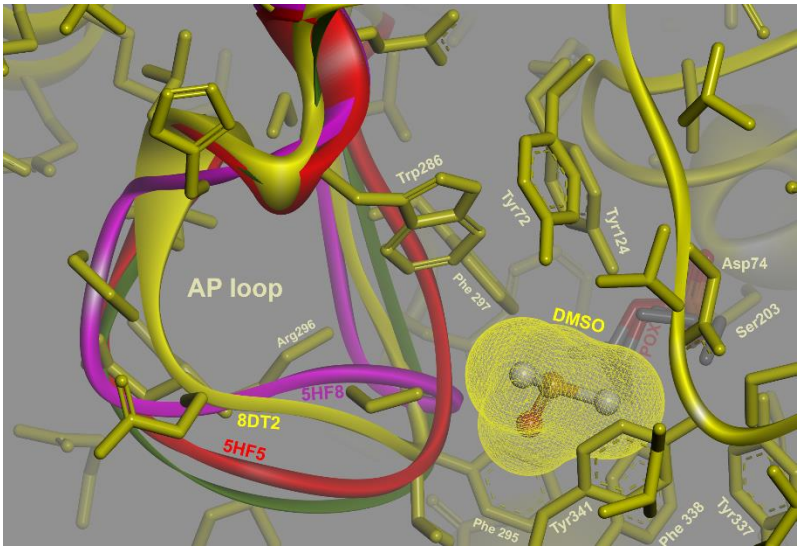

Figure 4. The acyl pocket loop (AP loop) conformations in the non-conjugated hAChE (green ribbon; PDB ID: 6U3P), POX-hAChE with DMSO (PDB ID: 8DT2; yellow), POX-hAChE without DMSO (PDB ID: 5HF5; red), POX-hAChE without DMSO (PDB ID: 5HF8; magenta). The hAChE backbone (in a ribbon), side-chains (in a stick) and molecule of DMSO (in a ball-and-stick and surface mesh) are all in yellow and represent X-ray structure of the POX-hAChE with bound DMSO (PDB ID: 8DT2).

Multitude of static AP-loop conformations in POX-hAChEs observed in X-ray structural data is also consistent with comparative inelastic neutron scattering (INS) analysis of the native and POX-inhibited hAChE [29] that identified the AP-loop of POX-hAChE as the most likely structural domain with significantly altered vibrational density of states as a consequence of the POX conjugation. It appears that binding of DMSO that could statically affect the AP-loop conformation would also have a chance to influence its conformational dynamics.

The analysis of PDB-deposited X-ray structures of VX-hAChE and POX-hAChE conjugates thus reveals significant conformational changes in the backbone and side-chains of the POX-hAChE centered in the AP loop, while no conformational changes have been observed in VX-hAChE conjugates (of the largely predominant S_P-VX-hAChE isomer). That structural information is consistent with our functional experiments of DMSO inhibition kinetics of hAChE (Fig.2) and bis-oxime reactivation kinetics of POX-hAChE and VX-hAChE (Fig.3.; Table 1).

It is possible that molecules of DMSO specifically bound in the active center gorge of POX-hAChE (Fig.4) stabilize one of conformations of the AP-loop that provides a better geometry for the bis-oxime stabilization, hence reduction in the K_{ox} values (Table 1). In that binding geometry, however, the ideal in-line attack of the oxime group, optimal for fast reactivation, was more difficult to achieve in the more compacted active-center volume of the larger POX-hAChE conjugate, compared to more spacious active center of the smaller VX-hAChE entity, hence reduction in k_2 values (Table 1).

The opposite effect on the K_{ox} for bis-oxime binding to VX-hAChE, the absence of the effect on k_2 values (Table 1) and the absence of associated conformational changes are all consistent with simple size-exclusion competition between DMSO and bis-oxime molecules.

3.3. X-ray structures of LG-1922 in reversible complexes with native hAChE and with POX-hAChE conjugate

We have solved X-ray structure of the reversible complex of the bis-oxime LG-1922 with POX-hAChE conjugate (Fig.5A) where DMSO was present. We found the nitrogen atom of the central substituted piperidine heterocycle of LG-1922 bound in direct apposition to Trp286 at a 3.6 Å distance providing a main stabilizing interaction and revealing, possibly, a cation-π interaction of the most likely protonated ~~heterocycle~~ piperidine (Fig. 5A). The shorter, two-methylene group oxime-bearing arm of the LG-1922 is directed to the opening of the active center gorge and bulk solvent without significant interactions with the enzyme, while its longer, three-methylene group arm extends towards the base of the gorge but reaching only half-way, up to the gorge constriction formed by Tyr124 and Tyr337, assuming a curled conformation stabilized by π-π interactions of its oxime group with 4.1 Å distant, aromatic ring of Tyr341. The oxime group oxygen points away from the 8.6 Å distant conjugated P atom of the POX in a clear non-productive orientation for the S_N2-type reaction.

The structure of LG-1922 bound to the native hAChE (Fig.5B) reveals nearly identical conformation of the bis-oxime. The central heterocycle, however, is shifted by 1.1 Å towards the base of the hAChE gorge, but slightly more pronounced curling of the lower oxime-bearing arm puts the oxime group to the identical position in both structures. Consequently, the distance between Trp286 and piperidine nitrogen of the LG-1922 increased by 0.5 Å to 4.1 Å in the LG-1922*hAChE complex, while the distance between the oxime group and Tyr341 remained at 4.1 Å.

The bis-oxime LG-1922 was synthesized as a racemic mixture with chiral center in the piperidine ring carbon where the shorter oxime-bearing arm is attached (Figs.1, 5, 6, and S1). Piperidine ring angle constraints that result in minimal geometric and conformational differences between the two enantiomers, as well as insufficient resolution of X-ray structures did not allow for distinction of the R from S isomers, determined by the puckering of the ring. Both enantiomers fit electron density equally well (Fig. S1), but only one enantiomer was used in the structure refinement due to low X-ray data resolution. Both, chiral carbon and the entire oxime-bearing arm face bulk solvent outside of the protein envelope of hAChE (Figs 5,6 and S1) and do not interact with enzyme residues. We therefore conclude that the chirality of the LG-1922 does not play a role in interaction with hAChE and POX-hAChE, and that in that context the compound behaves as an achiral molecule.

A molecule of DMSO is found in the choline-binding site of the LG-1922*POX-hAChE complex, harbored between Trp86 (at 4.7 Å) and one of the ethoxy substituents of conjugated POX-Ser203 (at 3.2 Å; Fig.5). At that position it can restrict rotational freedom of the ethoxy group and not allow it to assume fully extended conformation needed to open access to conjugated P atom for the incoming oxime group of LG-1922. In the structure of the LG-1922*hAChE complex, just like in the structure of POX-hAChE (PDB ID: 8DT2) DMSO was not found at that site, but rather a molecule of glycerol. This likely reflects an artifact of crystallographic procedure where glycerol at high concentrations is commonly used as the cryoprotectant in the flash-freezing of crystals in preparation for X-ray diffraction data collection at low, 100 K temperatures.

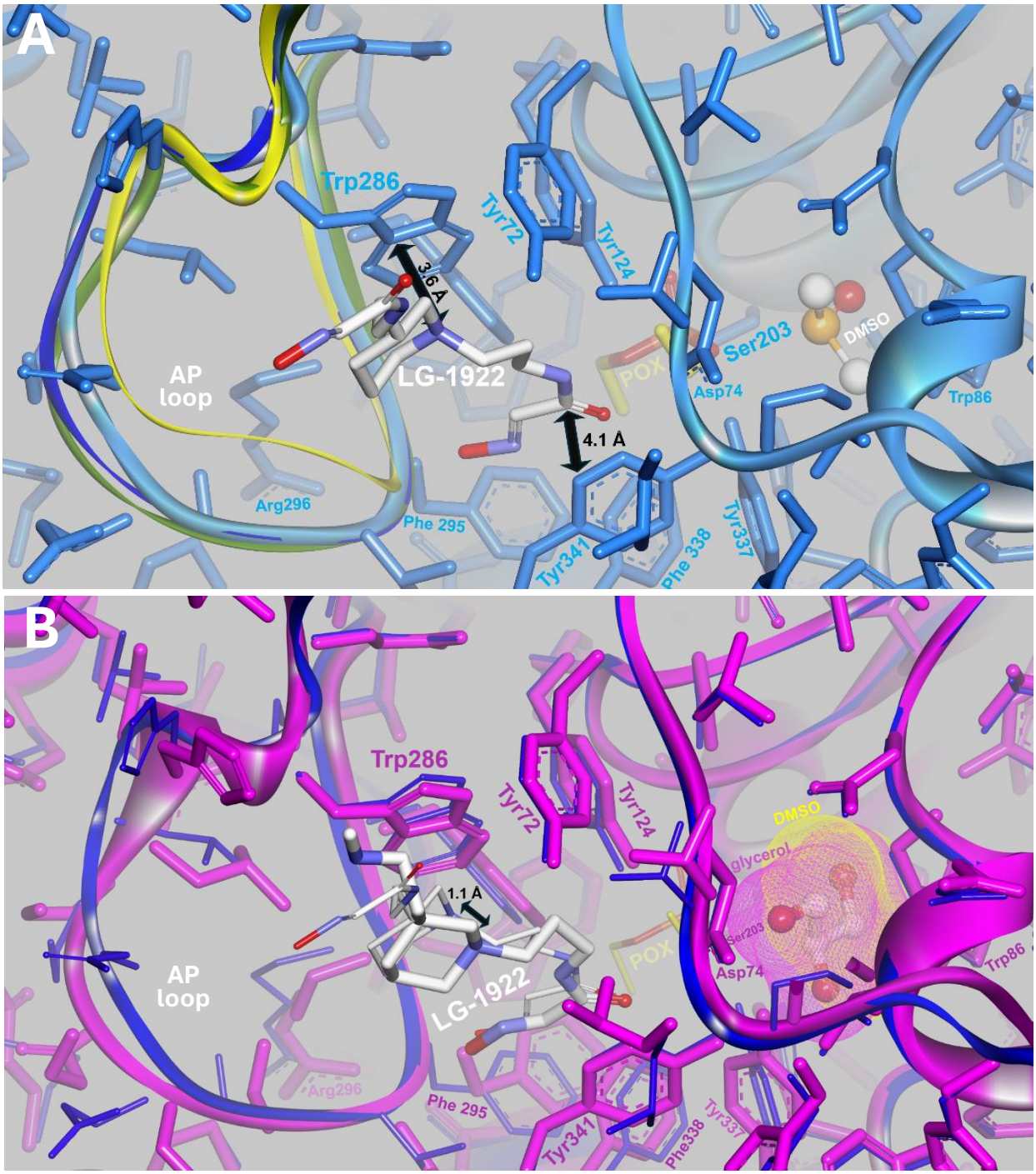

Figure 5. X-ray structures of the bis-oxime LG-1922 (white/blue/red sticks) in complex with hAChE. **A)** LG-1922*POX-hAChE complex (with DMSO at ~ 2 % present in the crystal; deposited to PDB as 9OMT). The conformation of the acyl pocket loop (AP loop) was slightly different in chains A (dark blue) and B (light blue) of the crystallographic homodimer. Conformations of the AP loop in the non-conjugated hAChE (PDB ID:6U3P; green) and in the POX-hAChE devoid of the bis-oxime (PDB ID:8DT2; yellow) were different as indicated. **B)** LG-1922* hAChE binary complex (in magenta ribbon and sticks), with glycerol was bound in the choline binding site, instead of DMSO (deposited to PDB as 9OMS). The structure from the panel A is superimposed (in blue ribbon and thin sticks). The central heterocycle of LG-1922 was shifted by 1.1 Å in the binary complex, but the lower oxime group held the same position as in the LG-1922*POX-hAChE structure in A.

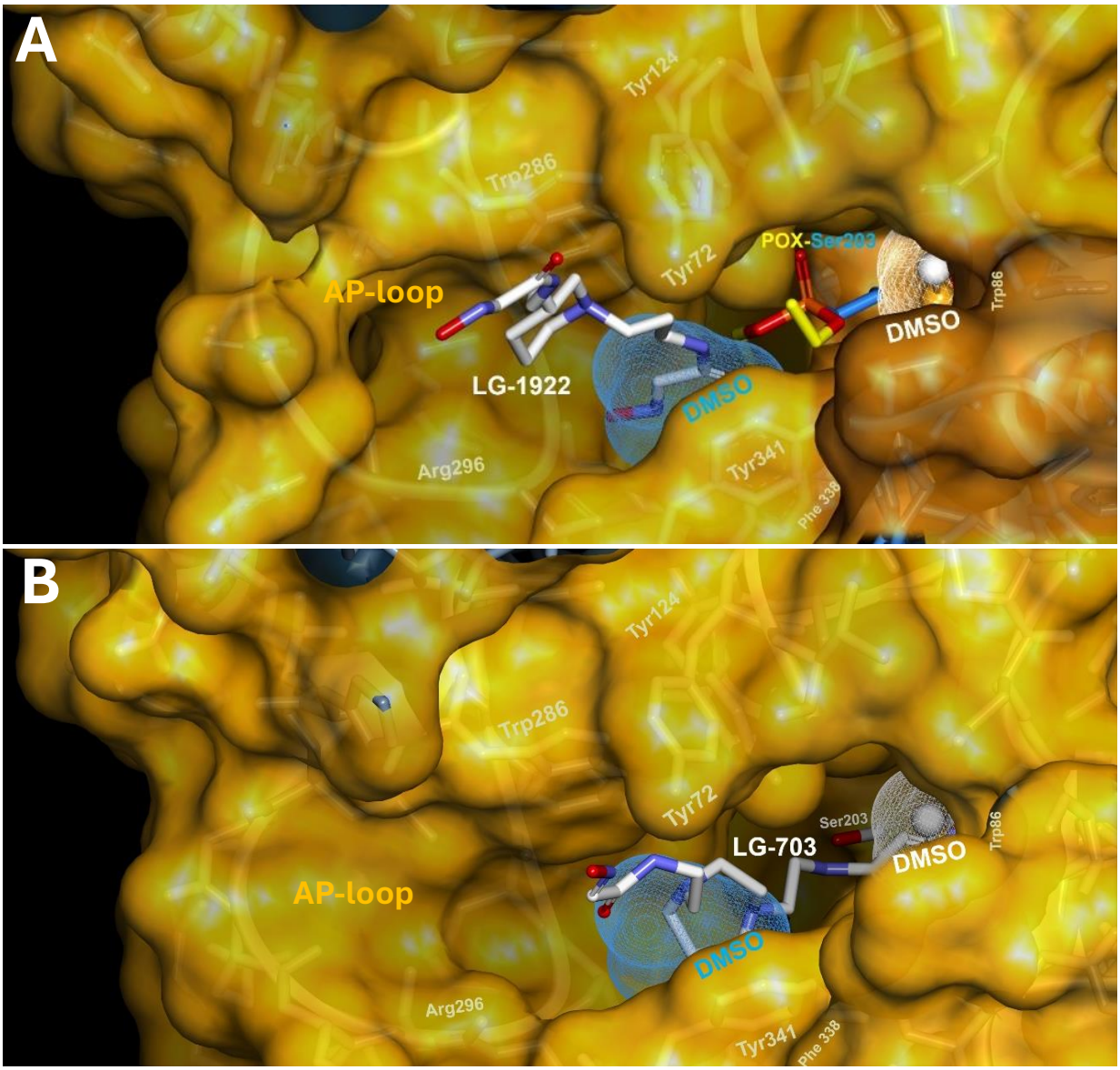

Figure 6. Sites of DMSO binding revealed in X-ray structures of heterocyclic bis-oximes LG-703 and LG-1922. Molecules of DMSO are represented as blue or white mesh and bis-oximes as sticks with C atoms colored white. A part of the hAChE Connolly surface (orange) is removed to expose the interior of the active center gorge. **A)** LG-1922 bound in the POX-hAChE (from Fig.5). A choline-binding site-bound DMSO found in the structure is in white mesh. A blue mesh DMSO is superimposed from the POX-hAChE structure 8DT2 (Fig.4). **B)** LG-703 bound in the non-conjugated hAChE (PDB ID: 6U3P: chain A). A white-colored DMSO is superimposed from the chain B of the same structure that contains no LG-703. A blue-colored DMSO is superimposed from the POX-hAChE structure 8DT2 (Fig.4).

In the LG-1922*POX-hAChE structure DMSO was not found at the opening of the active center gorge, next to the AP-loop (like in the PDB ID:8DT2) because this site was occupied by the longer arm of the LG-1922 molecule (Fig.6A). Molecule of DMSO was, however, found in the choline-binding site of the

LG-703*hAChE structure (PDB ID: 6U3P; Fig.6B), in the same location as DMSO in the LG-1922 structure.

Among all PDB-deposited X-ray structures of AChE, DMSO was found in only three: in the choline-binding site of 6U3P (chain B), next to the AP-loop in 8DT2 and in precisely the same position in the PDB ID: 4EY5, a reversible complex of hAChE with huperzine A [28]. Details of stabilization of DMSO in its two binding sites detected in hAChE reveal stabilization by aromatic Trps (86 and 286) and Tyrs (337 and 341), but also by anionic Glu202 and Asp74 (Fig.7). In the seven PDB-deposited X-ray structures (PDB IDs: 6QAA, 6R6W, 6SAM, 6QAC, 7AWG, 6QAB, 6QAD) of structurally related human butyrylcholinesterase (hBChE; EC 3.1.1.8) DMSO was also found, always in the choline-binding site next to Trp82 (equivalent of Trp86 in hAChE) in the location identical/superimposable to the one in the choline-binding site of hAChE. This was in spite of glycerol, bound elsewhere within the active center gorge of hBChE. The second binding site of DMSO found in hAChE, the one next to the AP-loop, was not observed in hBChE, most likely due to the difference in the AP-loop side-chain substituents in hBChE that results in larger opening of its active center gorge. The inhibitory effect of DMSO on catalysis of BChEs, seems to be less pronounced than in AChEs [9, 10]. We however note that a number of other deposited hAChE structures contains unmodeled electron density within the choline

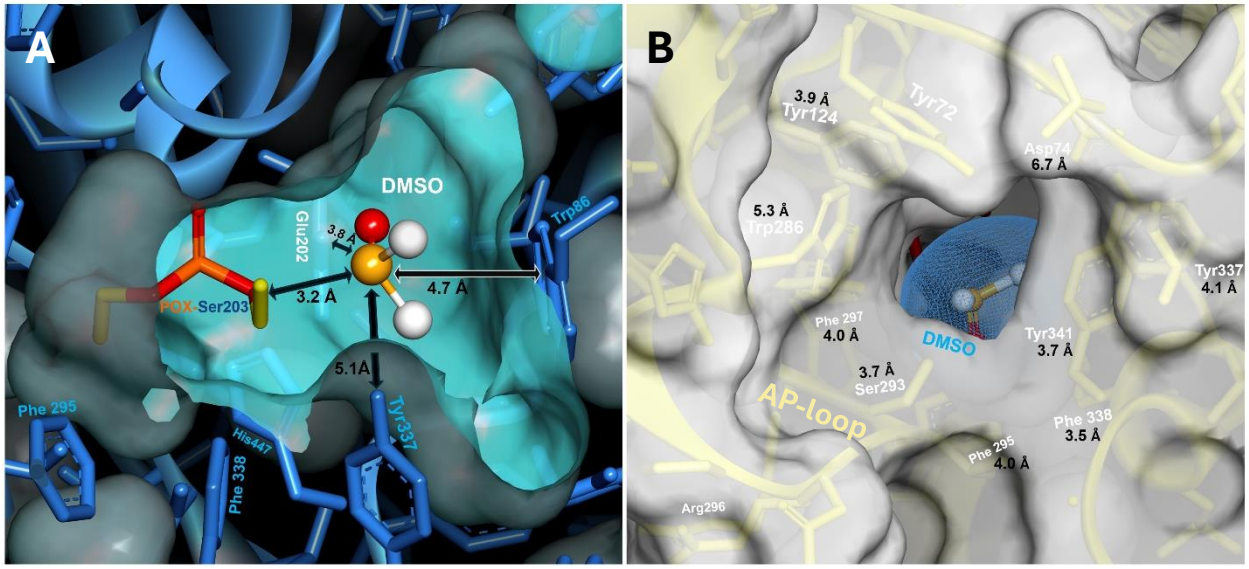

Figure 7. Details of two sites of DMSO (in ball-and-stick) binding to hAChE. **A)** Choline-binding site binding in the LG-1922*POX-hAChE complex (Fig.4). Nearly identical binding site of DMSO was found in the PDB ID 6U3P chain B. **B)** DMSO bound next to the AP-loop in the POX-hAChE structure 8DT2. The closest distances between atoms of DMSO and hAChE residues are given in black font. The blue mesh of DMSO illustrates a steric occlusion created at the active center gorge opening for the incoming bis-oxime molecules. Nearly identical binding site of DMSO was reported in the structure of the huperzine A*hAChE complex (PDB ID 4EY5).

binding site that can be interpreted as either DMSO or glycerol.

4. Conclusions

This functional and structural analysis of the interaction of solvent DMSO with hAChE and its conjugated forms, POX-hAChE and VX-hAChE, reveals two specific, concentration-dependent binding sites of DMSO in the active center gorge of hAChE. One is in the choline-binding site of hAChE and the other one at the active center gorge opening, next to the AP-loop of the enzyme.

DMSO inhibits ATCh turnover of hAChE in a competitive manner with K_i = 0.32 % or 45 mM (Fig.2A). It also largely competitively compromises reversible binding of heterocyclic bis-oximes, such as LG-703, in the same concentration range (Fig. 2B). Both effects are most likely due to DMSO binding in the choline-binding site, as suggested by structures of two mutually exclusive ligand complexes (LG-703*hAChE in the chain A and DMSO*hAChE in the chain B of the PDB ID: 6U3P).

DMSO binding also slows-down the reactivation kinetics of OP-hAChE conjugates, such as POX-hAChE and VX-hAChE, by uncharged heterocyclic bis-oximes, such as LG-703 and LG-1922, at an order of magnitude higher concentration range of DMSO (Fig.3). We are finding that the mechanism of DMSO interference depends on the nature of the OP-hAChE conjugate. For conjugates where conformation of hAChE (backbone and side-chains) is not changed by covalent binding of substituted phosphorus (such as VX-hAChE and most other OP-hAChEs) the slow-down is largely competitive in nature, resulting mainly in the increase of the K_{ox} constant (Table 1). The two-fold increase in the value of K_{ox} for VX-hAChE in 3 % DMSO for both tested bis-oximes suggests K_i^{DMSO} = ~3 % or ~400 mM, and it is possibly due to the DMSO binding next to the AP loop of hAChE as visualized in the X-ray structure of POX-hAChE (PDB ID: 8DT2) where DMSO was present at 2 % concentration [27]. Our X-ray structure of the bis-oxime LG-1922 in complex with POX-hAChE, however, reveals DMSO bound in the choline-binding site preventing LG-1922 to adopt an extended, productive orientation for reactivation (Fig.4) and resulting in the reduced rate constant $\boldsymbol{k_2}$, in a largely non-competitive type of effect (Table 1).

The two tested bis-oximes differ in the structure of their central heterocycles, sites of alkyl chain substitutions and in their length. It appears that the central homopiperazine of the LG-703, symmetrically substituted at 1,4 positions (unlike 1,3 substituted piperidine ring of LG-1922) results in 2-3-fold better reactivation efficiency of the VX- and POX-hAChE (Table 1). Nevertheless, the observed qualitative and quantitative effects of DMSO on their reactivation kinetics remain nearly the same (Fig. 3; Table 1).

These specific effects of DMSO become relevant in functional screening of novel, uncharged, potentially centrally active oxime reactivators of OP-hAChE that frequently exhibit limited solubility in the aqueous medium and where initial stock solutions need to be made in organic solvents, such as DMSO, that is easily carried over into medium for functional assays. The estimated efficacy of tested reactivators could be underestimated under those experimental conditions.

In addition, structural information obtained from X-ray structures in the presence of DMSO needs to be taken with some caution, due to potential for non-physiological artefacts associated with methodology of determination.

Acknowledgment

Crystallographic coordinates of the LG-1922*POX-hAChE complex and of the LG-1922*hAChE complex have been deposited to PDB as entries 9OMT and 9OMS, respectively.
X-ray crystallographic data were collected at Argonne National Laboratory using Structural Biology Center (SBC) beamline ID19 at the Advanced Photon Source. Use of the Advanced Photon Source, an Office of Science User Facility operated for the U.S. Department of Energy (DOE) Office of Science by Argonne National Laboratory, was supported by the U.S. DOE under Contract No. DE-AC02-06CH11357.
This research was supported by the CounterACT Program, NIH Office of the Director (OD), and the NINDS, [Grant Numbers 1U01NS083451, 1R21NS120839-01A2 and 1R21NS120884-01A2], and the UCSD AS award BG114128.

Conflict of interest

The authors declare that there are no conflicts of interest associated with this work.

Data availability

Data will be made available on request.

5. References

[1] C.M. Timperley, J.E. Forman, M. Abdollahi, A.S. Al-Amri, A. Baulig, D. Benachour, V. Borrett, F.A. Cariño, M. Geist, D. Gonzalez, W. Kane, Z. Kovarik, R. Martínez-Álvarez, N.M.F. Mourão, S. Neffe, S.K. Raza, V. Rubaylo, A.G. Suárez, K. Takeuchi, C. Tang, F. Trifirò, F.M. van Straten, P.S. Vanninen, S. Vučinić, V. Zaitsev, M. Zafar-Uz-Zaman, M.S. Zina, S. Holen, Advice on assistance and protection provided by the Scientific Advisory Board of the Organisation for the Prohibition of Chemical Weapons: Part 1. On medical care and treatment of injuries from nerve agents, Toxicology 415 (2019) 56–69, https://doi.org/10.1016/j.tox.2019.01.004

[2] J.E. Casida, Organophosphorus Xenobiotic Toxicology, Annu. Rev. Pharmacol. Toxicol. 57 (2017) 309–327, https://doi.org/10.1146/ANNUREV-PHARMTOX-010716-104926.

[3] L. Gorecki, O. Gerlits, X. Kong, X. Cheng, D.K. Blumenthal, P. Taylor, C. Ballatore, A. Kovalevsky, Z. Radić, Rational design, synthesis, and evaluation of uncharged, “smart” bis-oxime antidotes of organophosphate-inhibited human acetylcholinesterase, J. Biol. Chem. 295 (2020) 4079–4092, https://doi.org/10.1074/jbc.RA119.012400.

[4] L. Gorecki, A. Markova, V. Hepnarova, N. Zivna, L. Junova, M. Hrabinova, J. Janousek, T. Kobrlova, L. Prchal, D. Jun, O. Soukup, G. Horn, F. Worek, J. Marek, J. Korabecny, Uncharged mono- and bisoximes: In search of a zwitterion to countermeasure organophosphorus intoxication, Chem. Biol. Interact. 394 (2024) 110941, https://doi.org/10.1016/J.CBI.2024.110941.

[5] N. Maraković, A. Knežević, V. Vinković, Z. Kovarik, G. Šinko, Design and synthesis of N-substituted-2-hydroxyiminoacetamides and interactions with cholinesterases, Chem. Biol. Interact. 259 (2016) 122–132, https://doi.org/10.1016/j.cbi.2016.05.035.

[6] R.K. Sit, Z. Radić, V. Gerardi, L. Zhang, E. Garcia, M. Katalinić, G. Amitai, Z. Kovarik, V. V. Fokin, K.B. Sharpless, P. Taylor, New structural scaffolds for centrally acting oxime reactivators of phosphylated cholinesterases, J. Biol. Chem. 286 (2011) 19422–19430, https://doi.org/10.1074/jbc.M111.230656.

[7] J.P. Bennett, E.C. Meek, J.E. Chambers, Reactivation by novel pyridinium oximes of rat serum and skeletal muscle acetylcholinesterase inhibited by organophosphates, J. Biochem. Mol. Toxicol. 38 (2024) e23750, https://doi.org/10.1002/JBT.23750.

[8] J.E. Chambers, E.C. Meek, Novel centrally active oxime reactivators of acetylcholinesterase inhibited by surrogates of sarin and VX, Neurobiol. Dis. 133 (2020) 104487, https://doi.org/10.1016/J.NBD.2019.104487.

[9] A. Kumar, T. Darreh-Shori, DMSO: A Mixed-Competitive Inhibitor of Human Acetylcholinesterase, ACS Chem. Neurosci. 8 (2017) 2618–2625, https://doi.org/10.1021/acschemneuro.7b00344.

[10] N.A. Novales & J.P. Schwans, Comparing the effects of organic cosolvents on acetylcholinesterase and butyrylcholinesterase activity. Analytical biochemistry, 654 (2022) 114796, https://doi.org/10.1016/j.ab.2022.114796

[11] O. Fekonja, M. Zorec-Karlovsek, M. El Kharbili, D. Fournier, & J. Stojan, Inhibition and protection of cholinesterases by methanol and ethanol. Journal of enzyme inhibition and medicinal chemistry 22 (2007) 407–415, https://doi.org/10.1080/14756360601143857

[12] Z. Radić, R.K. Sit, Z. Kovarik, S. Berend, E. Garcia, L. Zhang, G. Amitai, C. Green, B. Radić, V. V. Fokin, K.B. Sharpless, P. Taylor, Refinement of structural leads for centrally acting oxime reactivators of phosphylated cholinesterases, J. Biol. Chem. 287 (2012) 11798–11809, https://doi.org/10.1074/jbc.M111.333732.

[13] O. Gerlits, K.Y. Ho, X. Cheng, D. Blumenthal, P. Taylor, A. Kovalevsky, Z. Radić, A new crystal form of human acetylcholinesterase for exploratory room-temperature crystallography studies, Chem. Biol. Interact. 309 (2019) 108698, https://doi.org/10.1016/j.cbi.2019.06.011.

[14] G.L. Ellman, K.D. Courtney, V. Andres, R.M. Featherstone, A new and rapid colorimetric determination of acetylcholinesterase activity, Biochem. Pharmacol. 7 (1961) 88–95, https://doi.org/10.1016/0006-2952(61)90145-9.

[15] W.N. Aldridge, E. Reiner, Enzyme inhibitors as substrates. Interactions of esterases with esters of organophosphorus and carbamic acids, North-Holland Pub. Co, Amsterdam, 1972.

[16] G. Amitai, R. Adani, O. Limanovich, S. Teitlboim, S. Yishay, L. Tveria, G. Yacov, H. Meshulam, L. Raveh, Characterization of asymmetric fluorogenic phosphonates as probes for developing organophosphorus hydrolases with broader stereoselectivity, Chem. Biol. Interact. 175 (2008) 249–254, https://doi.org/10.1016/j.cbi.2008.05.036.

[17] Z. Kovarik, Z. Radić, H.A. Berman, V. Simeon-Rudolf, E. Reiner, P. Taylor, Mutant Cholinesterases Possessing Enhanced Capacity for Reactivation of Their Phosphonylated Conjugates, Biochemistry 43 (2004) 3222–3229, https://doi.org/10.1021/bi036191a.

[18] W. Minor, M. Cymborowski, Z. Otwinowski, M. Chruszcz, HKL-3000: the integration of data reduction and structure solution--from diffraction images to an initial model in minutes, Acta Crystallogr., Sect. D, Biol. Crystallogr. 62 (2006) 859–866, https://doi.org/10.1107/S0907444906019949.

[19] M.D. Winn, C.C. Ballard, K.D. Cowtan, E.J. Dodson, P. Emsley, P.R. Evans, R.M. Keegan, E.B. Krissinel, A.G.W. Leslie, A. McCoy, S.J. McNicholas, G.N. Murshudov, N.S. Pannu, E.A. Potterton, H.R. Powell, R.J. Read, A. Vagin, K.S. Wilson, Overview of the CCP4 suite and current developments, Acta Crystallogr., Sect. D, Biol. Crystallogr. 67 (2011) 235–242, https://doi.org/10.1107/S0907444910045749.

[20] P.D. Adams, P. V. Afonine, G. Bunkóczi, V.B. Chen, I.W. Davis, N. Echols, J.J. Headd, L.W. Hung, G.J. Kapral, R.W. Grosse-Kunstleve, A.J. McCoy, N.W. Moriarty, R. Oeffner, R.J. Read, D.C. Richardson, J.S. Richardson, T.C. Terwilliger, P.H. Zwart, PHENIX: a comprehensive

Python-based system for macromolecular structure solution, Acta Crystallogr., Sect. D, Biol. Crystallogr. 66 (2010) 213–221, https://doi.org/10.1107/S0907444909052925.

[21] D. Liebschner, P. V. Afonine, M.L. Baker, G. Bunkoczi, V.B. Chen, T.I. Croll, B. Hintze, L.W. Hung, S. Jain, A.J. McCoy, N.W. Moriarty, R.D. Oeffner, B.K. Poon, M.G. Prisant, R.J. Read, J.S. Richardson, D.C. Richardson, M.D. Sammito, O. V. Sobolev, D.H. Stockwell, T.C. Terwilliger, A.G. Urzhumtsev, L.L. Videau, C.J. Williams, P.D. Adams, Macromolecular structure determination using X-rays, neutrons and electrons: recent developments in Phenix, Acta Crystallogr., Sect. D, Struct. Biol. 75 (2019) 861–877, https://doi.org/10.1107/S2059798319011471.

[22] V.B. Chen, W.B. Arendall, J.J. Headd, D.A. Keedy, R.M. Immormino, G.J. Kapral, L.W. Murray, J.S. Richardson, D.C. Richardson, MolProbity: all-atom structure validation for macromolecular crystallography, Acta Crystallogr., Sect. D, Biol. Crystallogr. 66 (2010) 12–21, https://doi.org/10.1107/S0907444909042073.

[23] P. Emsley, B. Lohkamp, W.G. Scott, K. Cowtan, Features and development of Coot, Acta Crystallogr., Sect. D, Biol. Crystallogr. 66 (2010) 486–501, https://doi.org/10.1107/S0907444910007493.

[24] A. Casañal, B. Lohkamp, P. Emsley, Current developments in Coot for macromolecular model building of Electron Cryo-microscopy and Crystallographic Data, Protein Sci. 29 (2020) 1069–1078, https://doi.org/10.1002/PRO.3791.

[25] Taylor, P., Hosea, N. A., Tsigelny, I., Radić, Z., & Berman, H. A. Determining ligand orientation and transphosphonylation mechanisms on acetylcholinesterase by Rp, Sp enantiomer selectivity and site-specific mutagenesis. *Enantiomer*, *2*(1997), 249–260.

[26] S.M. Bester, M.A. Guelta, J. Cheung, M.D. Winemiller, S.Y. Bae, J. Myslinski, S.D. Pegan, J.J. Height, Structural Insights of Stereospecific Inhibition of Human Acetylcholinesterase by VX and Subsequent Reactivation by HI-6, Chem. Res. Toxicol. 31 (2018) 1405–1417, https://doi.org/10.1021/acs.chemrestox.8b00294.

[27] O. Gerlits, X. Kong, X. Cheng, T. Wymore, D.K. Blumenthal, P. Taylor, Z. Radić, A. Kovalevsky, Productive reorientation of a bound oxime reactivator revealed in room temperature X-ray structures of native and VX-inhibited human acetylcholinesterase, J. Biol. Chem. 294 (2019) 10607–10618, https://doi.org/10.1074/JBC.RA119.008725.

[28] M.C. Franklin, M.J. Rudolph, C. Ginter, M.S. Cassidy, J. Cheung, Structures of paraoxon-inhibited human acetylcholinesterase reveal perturbations of the acyl loop and the dimer interface, Proteins 84 (2016) 1246–1256, https://doi.org/10.1002/PROT.25073.

[29] O. Gerlits, M. Fajer, X. Cheng, D.K. Blumenthal, Z. Radić, A. Kovalevsky, Structural and dynamic effects of paraoxon binding to human acetylcholinesterase by X-ray crystallography and inelastic neutron scattering, Structure 30 (2022) 1538-1549.e3, https://doi.org/10.1016/J.STR.2022.09.006.

[28] J. Cheung, M.J. Rudolph, F. Burshteyn, M.S. Cassidy, E.N. Gary, J. Love, M.C. Franklin, J.J. Height, Structures of human acetylcholinesterase in complex with pharmacologically important ligands, J. Med. Chem. 55 (2012) 10282–10286, https://doi.org/10.1021/JM300871X/SUPPL_FILE/JM300871X_SI_001.PDF.